Spatial chaos in weakly dispersive and viscous media: a nonperturbative theory of the driven KdV-Burgers equation.

M.A. Malkov [1]

Max-Planck Institut für Kernphysik, D-69029, Heidelberg, Germany

PACS: 47.52.+j, 52.35.Mw

Abstract

The asymptotic travelling wave solution of the KdV-Burgers equation driven by the long scale periodic driver is constructed. The solution represents a shock-train in which the quasi-periodic sequence of dispersive shocks or soliton chains is interspersed by smoothly varying regions. It is shown that the periodic solution which has the spatial driver period undergoes period doublings as the governing parameter changes. Two types of chaotic behavior are considered. The first type is a weak chaos, where only a small chaotic deviation from the periodic solution occurs. The second type corresponds to the developed chaos where the solution "ignores" the driver period and represents a random sequence of uncorrelated shocks. In the case of weak chaos the shock coordinate being repeatedly mapped over the driver period moves on a chaotic attractor, while in the case of developed chaos it moves on a repellor.

Both solutions depend on a parameter indicating the reference shock position in the shock-train. The structure of a one dimensional set to which this parameter belongs is investigated. This set contains measure one intervals around the fixed points in the case of periodic or weakly chaotic solutions and it becomes a fractal in the case of strong chaos. The capacity dimension of this set is calculated.

[1] to appear in Physica **D**
Email: Malkov@boris.mpi-hd.mpg.de

1 Introduction

Both the Korteweg de Vries (KdV) and the Burgers equations are widely used in the study of weakly nonlinear wave phenomena in a variety of continuous media. These equations have the same type of nonlinearity and represent dispersive and viscous system, respectively. In many realistic cases, however, both viscosity and dispersion are equally important (see eg.[1–3] and references therein) and a generalization of these two equations known as the Korteweg-de Vries -Burgers equation (KdVB) is very useful approximation to study the wave dynamics.

For wave motion to appear the equilibrium state of the system must be disturbed. Traditionally, this is attributed to initial conditions for the undriven equations. As far as the KdV and the Burgers equations are concerned, the time asymptotic behavior of the solution can often be described in terms of the dynamical evolution of fundamental solutions of these two equations, which are the cnoidal waves (the solitons in the limiting case) and the shocks for the KdV and for the Burgers equation, respectively (see e.g. [4,5]).

Different possibilities arise in the case of a continuously acting driver, which can be of an external or a growth rate type. The solutions of the undriven KdV and Burgers equations can also play a certain role when the driver is switched on. The driven equation itself, however, can possess a fundamental solution which is completely different from any solution of the undriven equation. Such a solution, called shock-train, has been proposed [6,7] in the framework of the so called derivative nonlinear Schroedinger-Burgers (DNLSB) equation, which is the viscous version of the DNLS-equation, introduced by Rogister, [8]. The idea behind this solution can be described as follows. In the case when both the dispersion and the viscosity are small, the solution is defined throughout most of the driver period by the balance between the nonlinear term and the driver. Since the nonlinearity of the equation provides more than one equilibrium state (two in case of the KdVB and three in case of the DNLSB equation, depending on the order of the nonlinear term), the overall solution can in principle be composed of the pieces of these different equilibria, connected by thin regions (shocks) where high derivative terms take part in the total balance. In terms of the ordinary differential equation (ODE) to which the original evolution equation is reduced when one is looking for the travelling wave solution, these shocks correspond to the transition between the unstable and stable types of equilibrium. Repeating this in the subsequent periods of the driver, we obtain a sequence of shocks, the shock train. Depending on the values of dispersion and viscosity each shock can be very oscillatory and can look more like a chain of solitons than a shock. The major difficulty here is to define the shock locations relative to the driver phase. This problem can be put in the following context. Suppose we know the location of the shock,

if any, within a given driver period which is equivalent to the specification of the boundary condition for the ODE. The question then is, where is the shock located within the neighbouring period? Provided that we can answer this question, the solution can in principle be calculated everywhere.

For the Burgers equation the answer is very simple: each shock must be at the same position relative to the driver phase, which yields a strictly periodic solution having the driver period [9]. This can be understood from Poincaré-Bendixson theorem in terms of the insufficient dimensionality of the related ODE. Indeed, the dynamical system that describes this travelling wave solution is two dimensional, and according to Poincaré-Bendixson theorem its attractors are limited by the fixed points and the limit circles. More extensive discussion of this issue and the relation to another type of solution that consists of choosing a stable branch of driver-nonlinearity equilibrium, can be found in [10]. The latter solution, containing no shocks at all has been constructed in [11] in the framework of the periodically driven KdV equation. In the present paper we demonstrate the possibility of a completely different response to an external force, giving rise to the formation of a shock-train. Moreover, this response seems to be more persistent, due to its ability to dissipate the pumped energy even at low viscosity, since shocks are involved.

Like other methods of description of complicated nonlinear systems, the shock-train technique outlined above can in principle produce physically irrelevant solutions. In particular, the shock train method reduces the continuous solution to a Poincaré map of the shock coordinate. This map is no longer constrained by the Poincaré-Bendixson theorem (even when the original dynamical system is) and in principle can falsify spatially chaotic behavior. Another danger is the possibility of the artificial temporal chaos caused by an insufficient number of modes in the computation of the shock train dynamics. For example such chaos has been observed during the numerical study of the unstably driven Burgers equation [10]. This observation is interesting in view of the remarkable and, after Lorenz's [13] famous paper widely exploited fact, that finite mode representation of continuous media can reveal chaotic behavior even for a very modest number of modes. In the case of shock-train dynamics the number of modes must be rather large to properly describe a shock structure at viscous and dispersive scales. The truncation virtually introduces the strong damping at the short scales which facilitates the appearance of stochastic attractor and rules out the shock-train, whereas the full solution (i.e. calculated with sufficiently large number of modes) shows that only regular shock-train dynamics occurs. Coming back to the possibility of spatial chaos, we note that the KdVB travelling waves are governed by the driven-damped nonlinear oscillator equation (see eq.(4) in the next section) which has a three dimensional phase space, and hence is not constrained by the Poincaré-Benidixson theorem in contrast to the Burgers equation.

A similar problem of spatial chaotization of periodically driven Alfven waves has been studied numerically in the framework of the DNLSB by Hada et al. [14]. In the present paper we turn to the KdVB equation which is a subset of the DNLSB and in its context describes weakly nonlinear oblique MHD waves. We also restrict ourselves to the case of small viscosity and dispersion, which is interesting for two reasons. First, this case corresponds to a quite typical situation in study of turbulence when the energy is pumped into a system at long scales, then transferred over an inertial range to short scales via nonlinear interaction of modes, and finally is dissipated there due to viscosity or any other short scale dissipation mechanism. Second, this case is difficult for numerical integration since different spatial scales appear. A direct manifestation of spatial chaos in the time dependent numerical study would formally require an infinitely large computation box or infinite number of modes.

The plan of the paper is as follows. In section 2 the shock-train solution to the KdVB equation within a driver period is obtained. In section 3 the solution from two neighbouring periods are matched. In section 4 the mapping of the shock coordinate at the driver period is introduced. In section 5 a route to chaos through the period doubling bifurcations is obtained as well as a developed chaos in the mapping of the shock coordinate is considered. Section 6 deals with numerical integration of the driven KdVB equation and compares the results.

2 Solution within one driver period

2.1 Overall behaviour

The KdVB equation that describes nonlinear waves, driven by a source moving with the constant velocity can be written in the following form

$$\frac{\partial u}{\partial t} + \frac{\partial}{\partial x}(u^2 - \lambda^2 u_{xx} - \mu u_x) = Q'(x). \tag{1}$$

We have transformed the coordinate system to the reference frame where a periodic driver

$$Q' \equiv dQ/dx$$

is at rest; u and x are normalized in such a way, that

$$Q(x + 2\pi) = Q(x),$$

and the function Q is of order unity whereas the dispersion coefficient λ^2 and the viscosity μ are both assumed to be small. We removed the linear term $c\frac{\partial u}{\partial x}$ from the l.h.s. of eq.(1) by shifting $u \to u - c/2$. From the physical point of view this choice of x and u variables corresponds to the case when the driver moves at the speed of a linear nondispersive undamped ($\lambda, \mu \to 0$) wave and, therefore, is in resonance with it. However, this does not mean the loss of generality, unless u is constrained by additional conditions like $x \to \pm\infty$ asymptotics. Note, that this particular constraint is relevant rather for the unforced case or for the case of localized forcing. In the case of periodic forcing, considered here a more suitable constraint is the mass invariant

$$\bar{u} = \frac{1}{2\pi n} \int_0^{2\pi n} u dx \tag{2}$$

that can be introduced for the $2\pi n$- periodic (n is integer) solution and is affected by the shift in u. In the above context Eq.(1) remains generic for all steady drivers unless $\bar{u}$ in Eq.(2)is specified. Below we specify explicitely a class of particular solutions of Eq.(1) considered throughout the most of this paper and we shall briefly return to their dependence upon the mass invariant (2) in sec.6, where these solutions are verified by the numerical integration of Eq.(1).

The nondispersive shock-train solutions do not allow the spatial chaotization, as it was stressed in the preceding section. We therefore consider the case of relatively strong dispersion

$$\mu \ll \lambda \ll 1 \tag{3}$$

when the developed oscillatory structures must appear nearby the shocks. At the same time, intending to obtain a solution with distinguished shocks in the shock-train we assume that those oscillations are appreciably damped between two shocks. The spatial damping rate of these oscillations is defined by μ/λ^2 and we assume that

$$\beta \equiv \mu/\lambda^2 \gtrsim 1. \tag{4}$$

Note, that under the conditions (3,4) an efficient method for Eq.(1) would be that one, developed by Whitham [15], and its generalization to the viscous driven case seems to be tractable. However, seeking the travelling wave solution of Eq.(1), which moves at the driver speed, i.e. assuming

$$\partial u/\partial t = 0,$$

we immediately arrive at the ODE which is the equation of the driven-damped nonlinear oscillator

$$u^2 - \lambda^2 u_{xx} - \mu u_x = Q(x). \tag{5}$$

Our analytical treatment in what follows will concern only (5), but we shall return to Eq.(1) in sec.6.

Interesting in the shock-train solutions of Eqs.(1) and (5), we choose the integration constant in the r.h.s. of (5), as

$$Q(x) = Q_0(x) + \lambda C_1 + \mu C_2 + \cdots, \tag{6}$$

where C_i are constants of order unity. According to the general shock-train method [9,10] these constants should be chosen in such a way, that $Q_0(x) \geq 0$ and Q_0, Q_0' go to zero simultaneously. This admits a pair of inviscid solutions $\pm\sqrt{Q_0}$ (to the leading order in λ and μ) and the smooth transition between them at points $x_0 \pmod{2\pi}$ where

$$Q_0(x_0) = Q_0'(x_0) = 0,$$

whereas each shock in the shocktrain is supposed to be somewhere between two such points.

To begin, we introduce the fast variable

$$\xi = \frac{1}{\lambda} g_1(x) + g_2 + \cdots, \tag{7}$$

where $g_i(x)$ are functions to be found from the further analysis. We seek the solution of (5) in the following form

$$u = u_0(\xi, x) + \lambda u_1 + \cdots. \tag{8}$$

Then, the first two orders of approximation yield

$$u_0^2 - g_1'^2 \frac{\partial^2 u_0}{\partial \xi^2} = Q_0 \tag{9}$$

$$2u_0 u_1 - g_1'^2 \frac{\partial^2 u_1}{\partial \xi^2} = 2g_1' g_2' \frac{\partial^2 u_0}{\partial \xi^2} + \left(\frac{\partial u_0}{\partial \xi}\right)^{-1} \frac{\partial}{\partial x} g_1' \left(\frac{\partial u_0}{\partial \xi}\right)^2 + \beta g_1' \frac{\partial u_0}{\partial \xi} + C_1 \tag{10}$$

The solution of Eq.(9) is a cnoidal wave (e.g. [4]), which depends on x as on a parameter. For convenience of the further analysis, we first represent it in the following form

$$u_0(\xi,x)=2\sqrt{Q_0}\left[\zeta_{-1}+(\zeta_0-\zeta_{-1})\mathrm{sn}^2\left(Q_0^{\frac{1}{4}}\sqrt{\frac{(\zeta_1-\zeta_{-1})}{3}}\frac{\xi}{g_1'},k\right)\right], \quad (11)$$

where ζ_n are the roots of the cubic equation

$$\zeta^3-\frac{3}{4}\zeta+\frac{a}{4}=0, \quad (12)$$

$$\zeta_n=\sin\left[\frac{1}{3}\arcsin a+\frac{2\pi n}{3}\right], \quad (13)$$

where $n=0,\pm1$, and k denotes the modulus of the elliptic function in Eq.(11)

$$k^2=\frac{\zeta_0-\zeta_{-1}}{\zeta_1-\zeta_{-1}}. \quad (14)$$

We have introduced the function $\mid a(x)\mid\leq 1$ or, equivalently, $0<k(x)\leq 1$ which is related to $a(x)$ by Eqs.(12-14), to be determined as a constant of integration of Eq.(9). In order to avoid the appearance of secular terms in the r.h.s. of Eq.(10), we specify $g_1(x)$ in such a way that the period of the solution $u_0(\xi,x)$ in ξ is independent of x. Then, the x-dependence of $\partial u_0/\partial\xi$ in the r.h.s. of Eq.(10) will not produce a nonperiodic in ξ term. Since

$$\zeta_1-\zeta_{-1}=\frac{3}{2}\frac{1}{\sqrt{k^2+k'^4}}, \quad (15)$$

we must set in Eq.(11)

$$g_1'=\frac{Q_0^{\frac{1}{4}}}{2^{\frac{3}{2}}\mathbf{K}(k^2+k'^4)^{\frac{1}{4}}}, \quad (16)$$

where $k'^2\equiv 1-k^2$ and $\mathbf{K}$ is the complete elliptic integral of the first kind. Eq.(11) then transforms to the following

$$u_0(\xi,x)=\sqrt{\frac{Q_0(x)}{k^2+k'^4}}\left[-1-k^2+3k^2\mathrm{sn}^2\left(2\mathbf{K}(k)\xi,k\right)\right] \quad (17)$$

To determine the function $k(x)$ we multiply Eq.(10) by $\partial u_0/\partial\xi$ and integrate over one period regarding x as a parameter. This yields the following simple

equation for $J(x)$

$$\frac{\partial J}{\partial x} + \beta J = 0, \tag{18}$$

where

$$J(x) = g_1' \int_0^1 \left(\frac{\partial u_0}{\partial \xi} \right)^2 d\xi. \tag{19}$$

Substituting Eqs.(16) and (17) $J(x)$ rewrites

$$J(x) = \frac{6\sqrt{2} Q_0^{5/4}(x)}{5(k^2 + k'^4)^{1/4}} \left[2\mathbf{E}(k) - \frac{k'^2(1+k'^2)}{k^2 + k'^4} \mathbf{K}(k) \right], \tag{20}$$

where $\mathbf{E}$ is the complete elliptic integral of the second kind. Eqs.(18) and (20) implicitly define the function $k(x)$ in the solution (17). Note, that the integration constants in the solutions of Eqs.(16) and (18) are not specified yet. It is convenient to attribute one of them to the shock coordinate x_* so that from Eqs.(7) and (16) we obtain

$$\xi \simeq \frac{g_1(x)}{\lambda} = \frac{1}{2^{3/2}\lambda} \int_{x_*}^{x} \frac{Q_0^{\frac{1}{4}} dx}{(k^2 + k'^4)^{\frac{1}{4}} \mathbf{K}(k)}. \tag{21}$$

The function $k(x)$ is defined by the following equation, which results from Eqs.(18) and (20)

$$\frac{Q_0^{\frac{5}{4}}(x) Q_0^{-\frac{5}{4}}(x_*')}{2(k'^2 + k^4)^{\frac{1}{4}}} \left[2\mathbf{E}(k) - \frac{k'^2(1+k'^2)}{k'^2 + k^4} \mathbf{K}(k) \right] = e^{-\beta(x - x_*')}, \tag{22}$$

where x_*' represents an arbitrary constant in the solution of Eq.(18), which we have specified in such a way that $k(x_*') = 1$, whereas $k(x_*) < 1$ (see Fig.1), and x_* is the nearest to the point x_*' root of the function $\partial u_0 / \partial \xi$. The solution (17) with $k(x)$ defined by Eq.(22) cannot be continued to the left from $x = x_*'$, since k exceeds unity in this region and (17) should be replaced there by a different solution (see Eq.(38) below). However, as we will see Eq.(17) yields the correct asymptotics in the region $x_*' - x \gtrsim \lambda$, provided that k is set to unity at $x < x_*'$. Therefore, we can define $k(x)$ for $x \in (x_0 - 2\pi, x_0]$ as follows

$$k = \begin{cases} k(x), & x_*' < x \le x_0 \\ 1, & x_0 - 2\pi < x \le x_*', \end{cases} \tag{23}$$

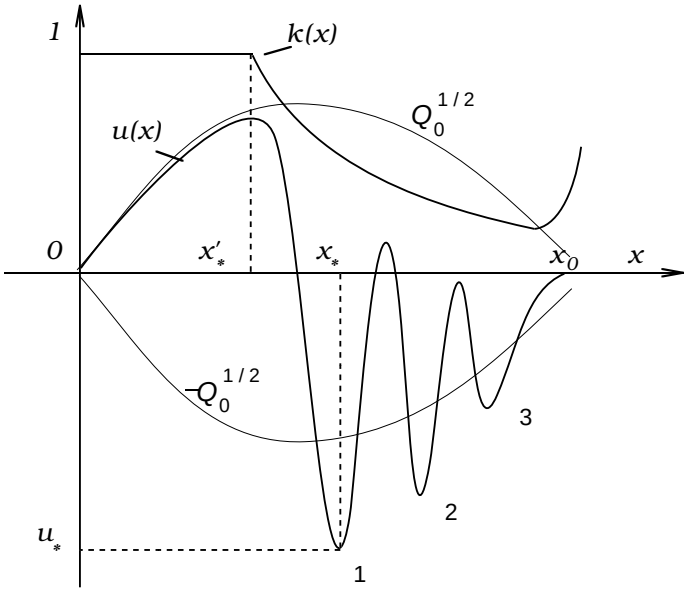

Fig. 1. An arrangement of the points x_* and x'_* in the zero order solution (17). Three solitons marked by digits fill up an interval between the shock front and the 'turning point' x_0. Inviscid nondispersive solutions $\pm Q_0^{1/2}$ are plotted with thin lines.

where $k(x)$ is the solution to Eq.(22) at $x > x'_*$. Indeed, since sn in Eq.(17) can be replaced in the region $x < x_*$ by tanh, (by virtue of $k'^2(x_*) \sim \sqrt{\mu/\lambda} \ll 1$, see Eq.(36) below) the solution u_0 tends to the unstable (for growing x) branch of the inviscid nondispersive solution of Eq.(5) $u \sim \sqrt{Q}$. At $x > x_*$ it oscillates around the stable branch $u \sim -\sqrt{Q}$, Fig.1. Not too far from the points $x_* \simeq x'_*$, i.e. at $x - x'_* < 1/\beta$, where $k(x)$ is still close to unity, these oscillations virtually form a soliton chain attached to the shock front to the right from x'_*. The number of these solitons is defined by the "optical length" between x_* and x_0. Beyond x_0 the oscillatory behavior of the solution is changed for the monotonic one (see the next section).

2.2 Resolving unsmooth region

Although the solution (17,23) is smooth in the fast variable ξ, it is not smooth in the slow variable x at $x = x'_* \simeq x_*$. The adiabatic approximation which allows the introduction of the fast and the slow variable breaks down there (the period of the solution in ξ tends to infinity near the separatrix $k = 1$), although the unsmoothness of $u_0(x)$ does not occur in the main order of approximation in $\lambda \ll 1$. A condition for the smooth matching of the solution at $x = x'_*$, where the derivative of $k(x)$ has a discontinuity, links the constants

x_* and x'_*. In order to do this matching we introduce the inner variable t in (5) defining it by

$$t = \frac{x - x_*}{\lambda}. \tag{24}$$

Eq. (4) then rewrites

$$u^2 - u_{tt} - \frac{\mu}{\lambda} u_t = Q(x_* + \lambda t). \tag{25}$$

Our nearest goal is to construct a part of the homoclinic (in terms of the slow variable x) orbit of Eq. (25) which tends to the solution (11) at large $|t| \gg 1$ for $\mid \lambda t \mid \ll 1$, and which is heteroclinic in fast variable t going from the saddle point to the stable focus (Fig.2). Introducing the "energy integral" of Eq.(25)

$$E = \frac{1}{2}u_t^2 - \frac{1}{3}u^3 + uQ(x_* + \lambda t) - \lambda \int Q'(x_* + \lambda t) u dt + \frac{\mu}{\lambda} \int u_t^2 dt \\ = \text{const}, \tag{26}$$

it is useful to evaluate Eq.(25) to the following integral for the function $t(u)$. To the first order of approximation in $\mu/\lambda \ll 1$ this function can be written down as

$$t = -\int_{u_*}^{u} \frac{du/\sqrt{2}}{\sqrt{E - uQ_* + \frac{1}{3}u^3 - \frac{\mu}{\lambda}\int_{u_*}^{u} u_t du}}. \tag{27}$$

Here $Q_* \equiv Q(x_*)$, $u_* \equiv u(t = 0)$ and the integral must be taken along the orbit with changing the branches of the square root at the turning points, according to the sign of u_t. The choice of the branches along the orbit can be understood with the help of Fig.2. We have omitted the terms of order of λ under the square root in (27) compared to μ/λ by virtue of our assumption $\lambda^2 < \mu$. Iterating Eq.(27) we substitute u_t from (26) at $\lambda, \mu/\lambda \to 0$ which yields for u_t as zeroth order solution of Eq.(27):

$$u_t^{(0)} = \sqrt{2}\sqrt{E - Q_* u + \frac{1}{3}u^3}. \tag{28}$$

Using normalized variable

$$\zeta = \frac{u}{2\sqrt{Q_*}}, \tag{29}$$

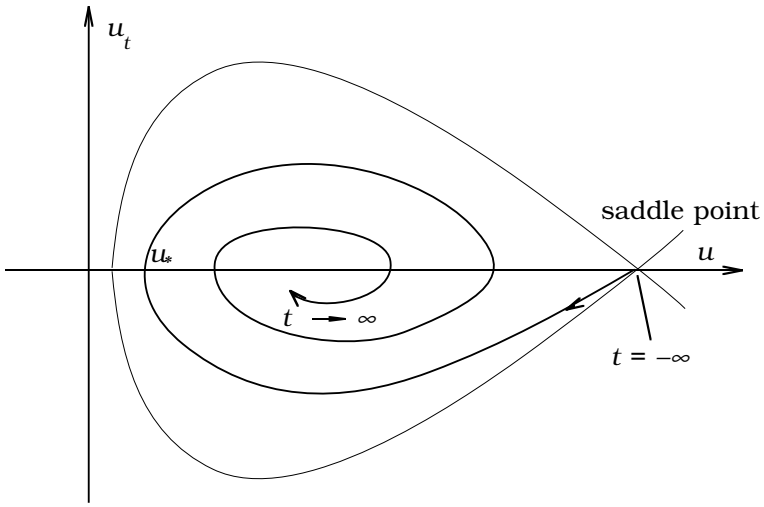

Fig. 2. Phase plane of Eq.(25)

instead of u and introducing

$$S = \frac{8}{\sqrt{3}} Q_*^{\frac{5}{4}} \int_{\zeta_*}^{\zeta} d\zeta \sqrt{\zeta^3 - \frac{3}{4}\zeta + \frac{a}{4}}, \tag{30}$$

from Eq.(27) we have as the second iteration (for negative t)

$$t(\zeta) = -\frac{\sqrt{3}}{2Q_*^{\frac{1}{4}}} \int_{\zeta_*}^{\zeta} \frac{d\zeta}{\sqrt{P(\zeta)}}. \tag{31}$$

Here

$$\zeta_* = \frac{u_*}{2\sqrt{Q_*}} = \zeta_{-1}(k_*),$$

where $k_* = k(x_*)$ and ζ_{-1} were defined by Eqs.(13,14) with

$$a = \frac{3E}{2Q_*^{\frac{3}{2}}},$$

$$P(\zeta) = \zeta^3 - \frac{3}{4}\zeta + \frac{1}{4}a + \frac{3}{8}\frac{\mu}{\lambda} Q_*^{-\frac{3}{2}} S(\zeta) \tag{32}$$

In order to be matched with the solution (11) at $t \to -\infty$, the solution $\zeta(t)$ of Eq.(31) must tend to the saddle point when $t \to -\infty$ (see Fig.2). This means that both $P(\zeta)$ and $dP/d\zeta$ must vanish at that point, which yields for the constant a

$$a \simeq 1 - \frac{18\sqrt{2}}{5Q_*^{\frac{1}{4}}}\frac{\mu}{\lambda}. \tag{33}$$

Together with the expansions at $k = k_* \simeq 1$

$$\zeta_* \equiv \zeta_{-1}(k_*) = -\frac{1}{2}\frac{1+k_*^2}{\sqrt{k_*'^2 + k_*^4}} \simeq -1 + \frac{3}{8}k_*'^4, \tag{34}$$

and

$$\zeta_{-1} = \sin\left(\frac{1}{3}\arcsin(a) - \frac{2\pi}{3}\right) \simeq -1 + \frac{1-a}{9}, \tag{35}$$

it defines the constant x_*' in Eq.(23) through the magnitude of $k'^2(x)$ at $x = x_*$, i.e through $k_*' \equiv k'(x_*)$, which is

$$k_*'^4 = \frac{16\sqrt{2}}{15}Q_*^{-\frac{1}{4}}\frac{\mu}{\lambda}. \tag{36}$$

Under this choice of x_*' the asymptotics of the solutions (17) at $\xi \to -\infty$ and (31) at $t \to -\infty$ do coincide. Indeed, at large negative t the main contribution to the integral (31) comes from the vicinity of the point $\zeta = 1/2$. Expanding $S(\zeta)$ at this point, so that

$$P(\zeta) = \left(\zeta - \frac{1}{2}\right)^2(\zeta - z), \tag{37}$$

where

$$z = -1 + \frac{3}{2^{3/2}Q_*^{1/4}}\frac{\mu}{\lambda}$$

and substituting then a from (33) for large negative t we obtain

$$t \sim -\frac{\sqrt{3}}{Q_*^{\frac{1}{4}}\sqrt{\frac{1}{2}-z}}\tanh^{-1}\sqrt{\frac{\zeta - z}{\frac{1}{2}-z}}. \tag{38}$$

Inverting this relation for $u(t)$ yields

$$u \sim 2\sqrt{Q_*}\left[z + \left(\frac{1}{2} - z\right)\tanh^2\left(\sqrt{\frac{1}{3}\left(\frac{1}{2} - z\right)}Q_*^{\frac{1}{4}}t\right)\right], \tag{39}$$

which is equivalent to the solution (11) or (17), taken at $k \simeq 1$ and $\mathbf{K}\xi$ in the argument of sn (see Eq.(17)) expanded at $x \simeq x_*$ to the same order of approximation.

Before we go to the extension of the solution to the neighbouring driver period, it is worthwhile to summarize the results of this section. Given the shock coordinate x_* we obtained the solution (17, 23), which is valid throughout one period of the driver. Besides x_*, the solution (17) depends on an additional constant x'_* (a point, where $k(x)$ approaches unity and the adiabatic approximation breaks down), which is connected with x_* through Eqs.(22) and (36). This solution, however, does not allow the straightforward continuation to the nearby period of the driver, since at $x = x_0$, where $Q_0 = 0$ the adiabatic approximation breaks down again. This region needs to be treated separately which provides the matching conditions for the solutions of the form (17) in the two neighbouring driver periods. Therefore, this matching creates a link between the two subsequent shock coordinates x_* and $\hat{x}_*$, which is the task of the next section.

3 Matching the solutions

In order to extend our solution beyond one driver period, let us turn now to the point $x = x_0$, where the type of equilibrium between the nonlinearity and the driver changes from the stable to unstable one. Since $u(x)$ tends to $-\sqrt{Q_0}$ with increasing $x - x_*$, we substitute

$$u = R + v \tag{40}$$

into (5), where $v(x)$ is supposed to be small, $R = \sqrt{Q_0}$ denotes the regular branch of the square root at $x = x_0$ which is positive at $x > x_0$ and is negative at $x < x_0$ (recall, that $Q_0(x) = Q'_0(x_0) = 0$). Then, linearizing (5) for small v, we obtain

$$2Rv - \lambda^2 v_{xx} - \mu v_x = \lambda^2 R_{xx} + \mu R_x + Q_1 + \cdots, \tag{41}$$

where we denoted the constant

$$Q_1 \equiv Q - Q_0 \sim \lambda$$

in Eq.(5). Introducing a new function

$$\phi = \exp\left[\frac{\beta}{2}x\right] v, \tag{42}$$

we get the following equation

$$\phi_{xx} - \left[\frac{2}{\lambda^2}R + \frac{\mu^2}{4\lambda^4}\right]\phi = F(x), \tag{43}$$

where $F(x)$ denotes

$$F(x) \equiv -\exp\left[\frac{\beta}{2}x\right]\left[\left(\frac{d}{dx} + \frac{\mu}{\lambda^2}\right)\frac{dR}{dx} + \lambda^{-2}Q_1\right]. \tag{44}$$

Since both λ and μ are small, one can show that to the leading order of approximation the solution of the Eq. (43) is defined by its homogeneous part, which can be written down asymptotically as

$$\phi(x) = \alpha\psi + \delta\chi, \tag{45}$$

where

$$\begin{aligned}\psi &= \frac{c}{p^{1/4}}\exp\left[\frac{1}{\lambda}S(x_1,x)\right],\\ \chi &= \frac{c}{p^{1/4}}\exp\left[-\frac{1}{\lambda}S(x_1,x)\right],\end{aligned} \tag{46}$$

and

$$S(x_1,x) = \int_{x_1}^{x}\sqrt{p}dx,$$

$$p = 2R + \frac{\mu^2}{4\lambda^2}, \quad p(x_1) = 0. \tag{47}$$

Here x_1 is the nearmost to x_0 zero of the function $p(x)$. The branches of $\sqrt{p}$ and constant c are chosen in such a way, that $\mathrm{Im}S > 0 \mid c \mid = 1$ on each Stokes line l_i, originating at the point x_1 and $\arg(cp^{-1/4}) \to 0$, $x \to x_1$, $x \subset l_i$ (Fig.3). Note, that we defined the Stokes lines l_i according to the condition $\mathrm{Re}S(x_1,x) = 0, x \subset l_i$. Given the shock coordinate x_* the asymptotic solution is known to the left from x_1, in particular on the line l_1. A convenient representation of it can be derived from Eq.(17) for $k \ll 1$:

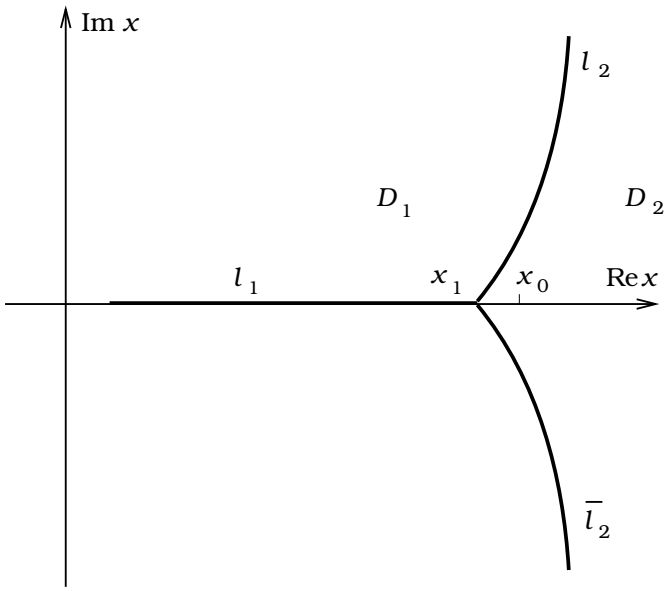

Fig. 3. The arrangement of the Stokes lines of Eq.(43)

$$u_0 \simeq -\sqrt{Q_0(x)} - 6\sqrt{\frac{2}{15\pi}}\frac{Q_0^{5/8}(x'_*)}{Q_0^{1/8}(x)}\exp\left[-\beta(x-x'_*)/2\right]\cos(2\pi\xi). \quad (48)$$

Here we have used the asymptotic solution of Eq.(22) for k^2 (x) in the region, where x satisfies the following two inequalities

$$\beta(x-x'_*) \gg 1,\ x_0 - x \gg \exp\left[-\frac{2}{5}\beta(x_0-x'_*)\right] \quad (49)$$

The latter restriction occurs since in the vicinity of the point $x = x_0$ the solution $k^2(x)$ of Eq.(22) starts to grow becoming invalid because $Q_0(x)$ approaches zero, as we noted earlier.

To make the further analysis more transparent in addition to the inequalities (3,4) we introduce the restriction $\mu^2 \ll \lambda^3$, which is, however, not a critical one, and, at the same time corresponds to the most interesting case of developed oscillatory structures near the shock fronts. Comparing Eq.(48) with eqs.(40), (42), and (45), which represents the WKB asymptotics to the left from the turning point x_1, we retrieve α and δ in Eq.(45)

$$\alpha = -2^{3/4}\sqrt{\frac{3}{5\pi}}Q_0^{5/8}(x'_*)\exp\left[\beta x'_*/2 - 2\pi i P_1/\lambda\right]$$

$$\delta = \bar{\alpha}, \quad (50)$$

where the bar denotes complex conjugate and

$$P_1 = \int\limits_{x_*}^{x_1} \frac{Q_0^{1/4} dx}{2^{3/2}\mathbf{K}(x)(k^2 + k'^4)^{1/4}}. \tag{51}$$

In our above calculations of the coefficients α and β we have extended the asymptotic solution (48) up to the point $x = x_1$ (see Eq.(51)). If, however, $x_0 - x_1 \lesssim \exp\left[-\frac{2}{5}\beta(x_0 - x'_*)\right]$, which can be the case for relatively small $x_0 - x'_*$ (note that $x_0 - x_1 \sim \mu^2/\lambda^2 \ll 1$), the solution (48) together with the solution (11) becomes invalid and should be replaced by the solution which was obtained in this section for the vicinity of the turning point $x = x_1$ (eqs.(40), (42), and (45)). According to this modification, the integrand in the phase integral (51) should be taken with $k^2(x) = 0$ in this region. This correction might become quantitatively important in calculation of the shock map for x_* approaching x_0 (see ineq.(49)), which will be taken into account in the next section.

The asymptotic solution to the right from $x = x_1$ can be obtained by making use of the standard WKB approximation, which links the coefficients α, δ in the sectors D_1 and D_2 (see e.g. [16]). In the region D_2 the solution reads

$$\phi = \alpha_2 \psi + \delta_2 \chi \tag{52}$$

with

$$\alpha_2 = e^{-i\pi/3}(\alpha + i\bar{\alpha}) \tag{53}$$

and

$$\delta_2 = ie^{-i\pi/3}\alpha. \tag{54}$$

Thus, a solution, which is valid also for real $x > x_1$ can be written in terms of the function $v(x)$ (Eq.(40)) as

$$v(x) = 2^{-1/4} R^{-1/4}(x) e^{-\beta x/2 - i\pi/4} \left[(\alpha + i\bar{\alpha}) e^{S(x_1,x)/\lambda} + i\alpha e^{-S(x_1,x)/\lambda}\right]. \tag{55}$$

Taking $\mu^2 \ll \lambda^3$ into account, after a simple algebra from the last equation we obtain

$$u(x) = R - \sqrt{\frac{6}{5\pi}} \frac{Q_0^{\frac{5}{8}}(x'_*)}{Q_0^{\frac{1}{8}}(x)} e^{-\beta(x - x'_*)/2}\,.$$

$$\cdot \left[2\cos\left(\frac{2\pi}{\lambda}P_1 + \frac{\pi}{4}\right) \exp\left(\frac{\sqrt{2}}{\lambda}\int\limits_{x_1}^{x} Q_0^{\frac{1}{4}}\,dx\right)\right.$$
$$\left. + \exp\left(\frac{i\pi}{4} - \frac{2i\pi}{\lambda}P_1 - \frac{\sqrt{2}}{\lambda}\int\limits_{x_1}^{x} Q_0^{\frac{1}{4}}\,dx\right)\right]. \qquad (56)$$

Now we can construct the solution in the region $x_0 < x < x_0 + 2\pi$. Suppose the next shock is located at $x = \hat{x}_* + 2\pi$, so that we take all the subsequent shock coordinates $x \pmod{2\pi}$. Our task is to link $\hat{x_*}$ with x_*, which defines by an induction the solution for all $x > x_*$. According to Sec.2, the solution, which is valid in the region $x_0 < x < x_0 + 2\pi$, but not too close to the end points of this interval can be written in the form (17), with $\hat{x}_*$ instead of x_* in (21). Then, taking (11) at large negative ξ, i.e. using Eq.(39) with $\hat{x}_*$ instead of x_*, we obtain

$$u(x) \simeq \sqrt{\hat{Q}_*}\left\{1 - 12\exp\left[\frac{2}{\sqrt{3}}\sqrt{\frac{1}{2} - \hat{\zeta}_*}\hat{Q}_*^{\frac{1}{4}}\frac{x - \hat{x}_* - 2\pi}{\lambda}\right]\right\}. \qquad (57)$$

Here we introduced the notations $\hat{Q}_* \equiv Q(\hat{x}_*)$ and $\hat{\zeta}_* \equiv \zeta_*(\hat{x}_*)$, whereas the function $\zeta_*(x_*)$ is defined by Eq.(34). Expanding $\hat{\zeta}_*$ at small μ/λ yields

$$u \simeq \sqrt{\hat{Q}_*} - 12\sqrt{\hat{Q}_*}\exp\left[\sqrt{2}\hat{Q}_*^{1/4}\frac{x - \hat{x}_* - 2\pi}{\lambda} - \beta(x - \hat{x}_* - 2\pi)/2\right]. \qquad (58)$$

This asymptotic solution should be matched with the asymptotics (56) in the region where they both are valid. This region is defined by the following two inequalities

$$\lambda \ll \hat{x}_* + 2\pi - x \ll \hat{x}_* + 2\pi - x_0,$$

To match Eqs.(56) and (58) we can evaluate the integral in Eq.(56) as follows

$$\int\limits_{x_1}^{x} Q_0^{1/4}dx \simeq \int\limits_{x_1}^{\hat{x}_*+2\pi} Q_0^{1/4}dx - \hat{Q}_*^{1/4}(\hat{x}_* + 2\pi - x).$$

The asymptotic solutions (56) and (58) will coincide in the region of their validity if the following condition is met

$$\frac{Q_0^{5/8}(x'_*)}{\sqrt{30\pi}\hat{Q}_*^{5/8}}\cos\left(\frac{2\pi}{\lambda}P_1 + \frac{\pi}{4}\right)\cdot$$

$$\cdot \exp\left[-\frac{\beta}{2}(\hat{x}_* + 2\pi - x'_*) + \frac{\sqrt{2}}{\lambda}\int\limits_{x_1}^{\hat{x}_*+2\pi} Q_0^{1/4} dx\right] = 1. \tag{59}$$

4 Mapping the shock coordinate

4.1 Arbitrary 2π- periodic driver

Equation (59) provides an implicit relation between the two subsequent shock coordinates x_* and $\hat{x}_*$. However, it is still rather complex for a comprehensive analysis. First of all there are two intermediate coordinates x'_* and x_1 in Eq.(59) that appeared during the evaluation of the map $x_* \mapsto \hat{x}_*$. They have no other physical meaning than x_* and x_0 already do. Given the shock coordinate x_*, the value x'_* can in principle be calculated by means of Eqs.(22) and (36), whereas x_1 is defined by Eq.(47) and lies close to the point x_0. Moreover, our assumption $\mu^2 \ll \lambda^3$ allows us to replace x'_* by x_* and x_1 by x_0, respectively (see Eqs.(22), (36) and (47)). We can also set $x_0 = 2\pi$ without loss of generality. After these simplifications we rewrite the map $x_* \mapsto \hat{x}_*$ as

$$f(x_*) = g(\hat{x}_*), \tag{60}$$

where

$$f(x) = Q_0^{5/8}(x)\cos\left[\frac{\pi}{\sqrt{2}\lambda}\int\limits_x^{2\pi}\frac{Q_0^{1/4}dx}{\mathbf{K}(x)(k^2+k'^4)^{1/4}} + \frac{\pi}{4}\right]e^{\beta(x/2-\pi)}, \tag{61}$$

and

$$g(x) = \sqrt{30\pi}Q_0^{5/8}(x)\exp\left[-\frac{\sqrt{2}}{\lambda}\int\limits_0^x Q_0^{1/4}dx + \frac{\beta x}{2}\right]. \tag{62}$$

4.2 Sinusoidal driver

Let us consider the simplest case of sinusoidal driver in Eq.(1):

$$Q' = \frac{1}{2}\sin(x) \tag{63}$$

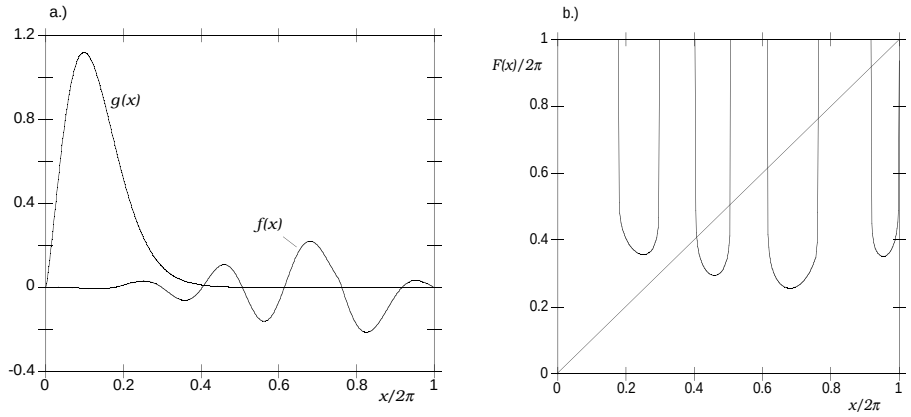

Fig. 4. a.) The functions $f(x)$ and $g(x)$ b.) The map of the shock coordinate $F(x)$

Then, according to Eq.(6) and the text right after it we have for Q_0

$$Q_0 = \sin^2 \frac{x}{2},$$

The functions f and g are shown in Fig.4a. One can see, that given x_*, Eq.(60) can not be uniquely resolved for $\hat{x}_*$, since there are two different x for each $g(x)$. At the same time, the function $g(x)$ at $x < x_m$ (the point of maximum of function $g(x)$) corresponds to the position of the next shock $\hat{x}_*$, which is too close to x_0 to be correctly described by our approximation, since the asymptotic method of the derivation of the map $x_* \mapsto \hat{x}_*$ implies, that $\hat{x}_* \gg \lambda$. Indeed, $x_m \sim \lambda^{2/3}$ and the solution with $\hat{x}_* < x_m$ can hardly satisfy the inequality $\hat{x}_* \gg \lambda$ except for very small λ. In general, this solution would correspond to the shockless one, which stays at the stable equilibrium $u \sim -\sqrt{Q}$ after the phase of the driver advanced beyond the point x_0 (the jump would be of the order of $x_m - x_0 \ll 1$) and the matching should be treated on different basis. The above nonuniqueness is important when considering Eq.(5) per se. Here, we are looking for the travelling wave solutions of Eq.(1) and any particular choice of solution is justified. Interested in the shock-train solutions we choose $\hat{x}_* \in [x_m, 2\pi]$ for $g(\hat{x}_*)$ from Eq.(60). In this case the mapping $x_* \mapsto \hat{x}_*$ is unique, although it is not defined for x, where

$$f(x) < \min_{x \in [x_m, 2\pi]} g(x) \tag{64}$$

as well as in the interval $[0, x_m)$. Resolving Eq.(60) numerically and omitting stars at x we get the mapping $F(x) : x \mapsto \hat{x}$, which is shown in Fig.4b.

5 Simple solutions of period one and the period-doubling bifurcations

5.1 Weak chaos

As discussed in the preceding section, the map [1] $F(x)$ (Figs.4) is not defined in those intervals where the inequality (64) is met. This means that after an iterate of the map $F(x)$ has fallen into one of these intervals (denote them $J_{\rm k}$, and include also $[0, x_{\rm m})$ in this category, as we have mentioned above), the travelling wave solution of the shock-train type cannot be continued to the right from this point. At the same time, a continuous to the zeroth order (in λ and μ) solution could in principle be constructed in this driver period, as it was described in sect.1. However, we leave aside this possibility and restrict our consideration to the shock-trains. According to Eq.(60), the total number of intervals where $F(x)$ is defined, can be estimatd as $N_{\rm I} \sim 1/\lambda \gg 1$. We denote these intervals as $\{I_k\}_{k=1}^{N_{\rm I}}$. The number of the fixed points of the map $F(x)$ is $N_{\rm F} \lesssim 2N_{\rm I}$. Each fixed point of $F(x)$ corresponds to 2π -periodic solution of Eqs.(1) and (4). Since at a fixed point x

$$\mid dF/dx \mid = \frac{f'(x)}{g'(x)} \sim \exp\left[\frac{\sqrt{2}}{\lambda}\int\limits_0^x Q_0^{1/4} dx\right] \gg 1, \qquad (65)$$

these fixed points are mostly unstable with a possible exception for a point, where $g(x)$ is not very small, or where $f(x)$ reaches its maximum. Accordingly, the one parameter (x_*) family of solutions of Eq.(5), constructed in the previous section with x_* taken to be equal to one of this fixed points represents an unstable periodic orbit of Eq.(5). It is important to note here, that the unstable in x periodic solution of Eq.(5) can correspond to the stable (in time) periodic travelling wave solution of the driven KdVB Eq.(1). This will be demonstrated in sec.6. We also note, that the instability of a fixed point evolves in the positive x-direction, whereas the same fixed point attracts the backward iterations of the Poincaré section even though the map has no unique inversion. The question how the spatial stability of our periodical solition is related to its temporal stability deserves a special treatment which is beyond the scope of this paper. Note, that even in linear systems the answer can be not a straightforward one (e.g. absolute versus convective instability in plasmas).

We begin our analysis of the map $F(x)$ with the case when a minimum of $F(x)$ is close to one of its fixed points, say $x = a$, (Fig.5). In this case the local behavior of the iterates near this fixed point does not differ from that which is known for one dimensional map with one maximum [17]. In particular,

[1] In what follows we relate $x, F(x)$ to the interval $[0, 1]$ instead of $[0, 2\pi]$.

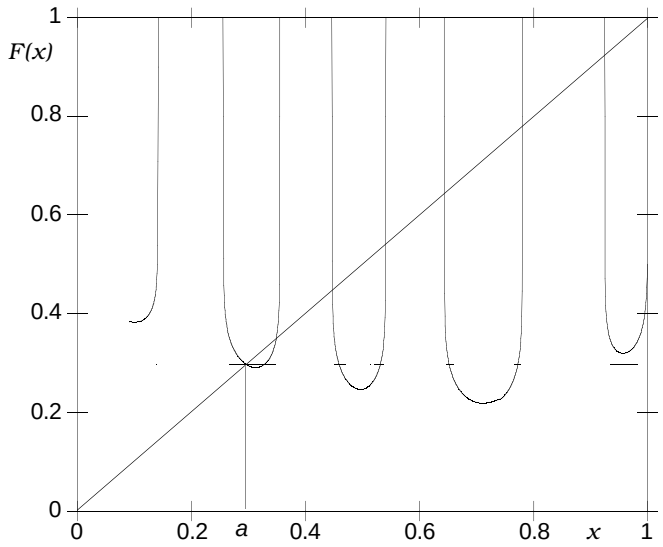

Fig. 5. Mapping of the shock coordinate with one stable fixed point $x = a$ for $\lambda = 0.27$ and $\beta = 1.2$. Horisontally aligned points, which are generated by $F^{100}(x)$, actually mark the basin of attraction of this fixed point

starting with the stable fixed point $x = a$, $\mid F'(a) \mid < 1$, we obtain a series of period doubling bifurcations when, for instance, λ is fixed $\lambda = 0.27$ while β changes from $\beta = 1.2$ down to $\beta = 0.98$ (see Fig.5-7). Below the point $\beta = 0.98$ the local behavior of the mapping $F(x)$ becomes chaotic. At the tangential bifurcation of the fixed point one can observe an intermittent behavior of the mapping [18], although the return time to the vicinity of the tangent point (where $F(x) - x \ll x$) might be quite large, since the orbit visits many other intervals of the mapping $F(x)$ before it finds the return path, if ever. The measure one basin of attraction of the fixed point $x = a$ and emerged 2^n cycles is made up of the points which are under the horizontal lines seen in Figs.5-6 and under the scattered points shown in Figs.7. When we start to iterate $F(x)$, with an initial point from the basin of attraction the iterations will be attracted by the fixed point or will be trapped in 2^n cycle which is the fixed point of the map F^n defined by $F^n = F \circ F^{n-1}(x)$; $F^0(x) \equiv x$. Almost all other points of the $[0, 1]$ interval will sooner or later escape in one of the intervals J_k where $F(x)$ is not defined. This means that for almost all initial shock coordinates which are not from the basin of attraction, the shock-train solution can not be continued infinitely into the positive x-direction. The rest (a measure zero subset) of the $[0, 1]$ interval, which we meant by saying "almost all" will be considered in the next section. It is worth noting, that although the measure zero solutions are exceptional for the ODE (5), they can be very

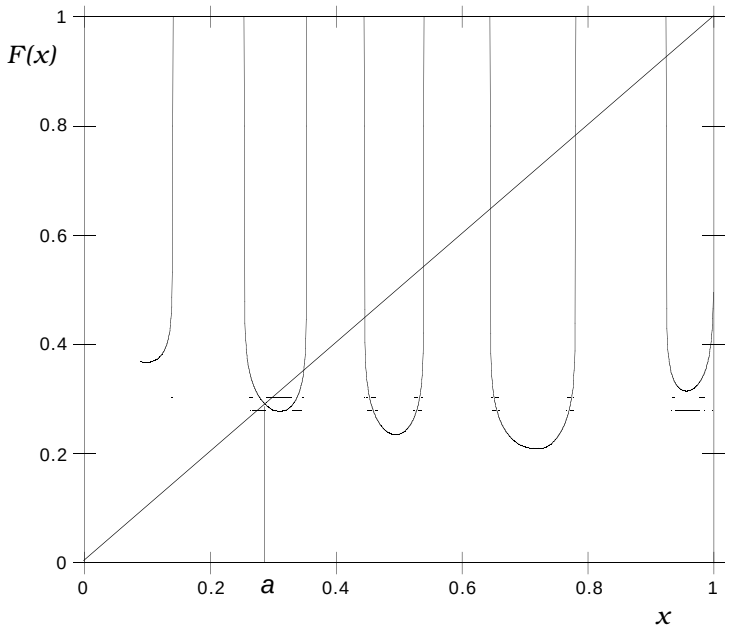

Fig. 6. Stable cycle of period 2 near the fixed point a, $\lambda = 0.27$, $\beta = 1.1$. The 100-th ($F^{100}(x)$) iteration is shown as well as $F(x)$

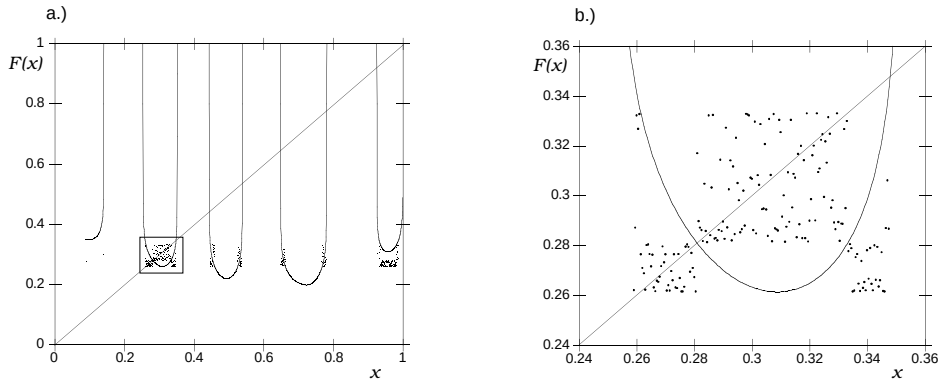

Fig. 7. a.) The same as in Fig.6 but for $\beta = 0.98$ b.) A magnification of the box in Fig.7a.

persistent and quite "typical" travelling wave solutions of the correspondent evolution equation Eq.(1).

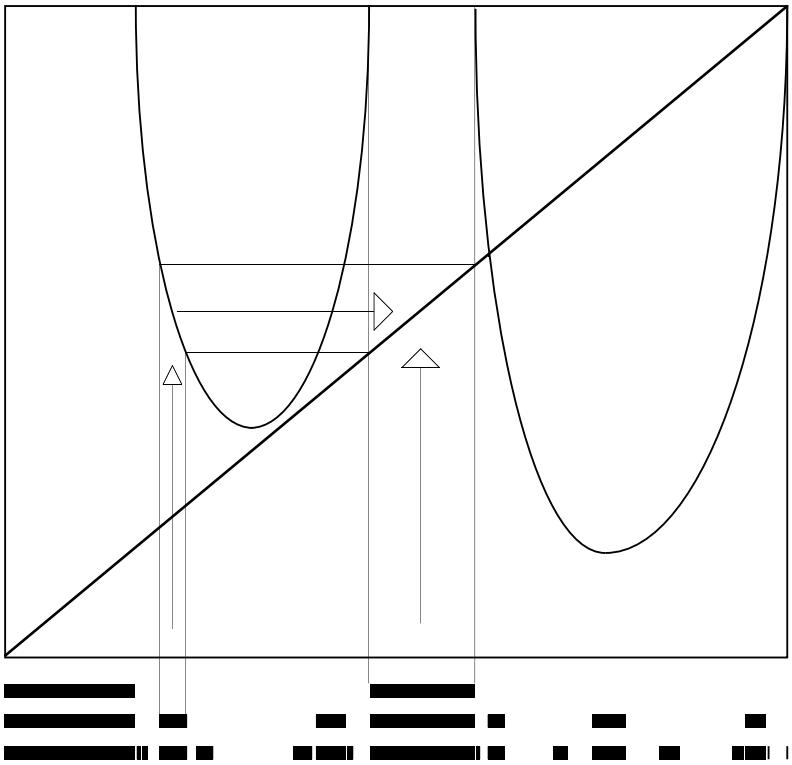

Fig. 8. A piece of the map $F(x)$ illustrating the fragmentation of phase space under iterations. The points from the black areas will escape as it is shown by the arrows.

5.2 Strong spatial chaos

The behavior of the iterates considered in the previous section is chaotic for β below $\beta_c = 0.98$, but this chaos is weak in the sense that the spatial profile of the solution of Eq.(1), corresponding to this sequence of shock coordinates $\{x_n\}_{n=0}^{\infty}$ is still rather close to periodic solution since $\mid x_n - a \mid \lesssim \lambda$. By further decreasing of β, the measure one basin of this weakly chaotic attractor around $x = a$ disappears, and almost all initial points will escape in $[0,1] \setminus \bigcup_{k=1}^{N_I} I_k$ as it was argued in the previous subsection. To identify the nonwandering points of F which define now the sequence of shocks in the spatially chaotic solution of Eq.(1), we proceed as follows. Consider the nonescape set, which occurs under the backward iterations of $\bigcup_{k=1}^{N_I} I_k$ and denote its limit by $A = [0,1] \setminus \bigcup_{n=0}^{\infty} F^{-n}\left(\bigcup J_k\right)$, (recall, that J_k denotes the escape intervals). The construction of this set is similar to that of the classical Cantor set and is illustrated in Fig.8. Once the initial shock coordinate is taken from the set A, the shock train solution can be continued ad infinitum.

An important property of this set is its capacity dimension. One calculates it

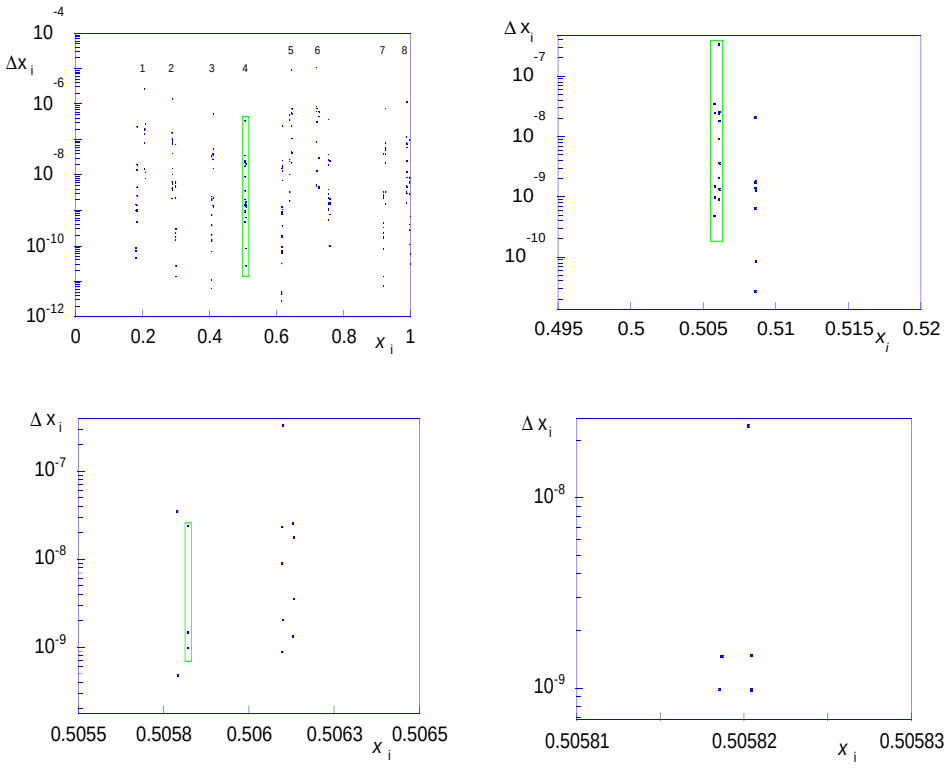

Fig. 9. Illustration of the natural measure of chaotic repellor of the map $F(x)$. All four plots show the lengths of intervals that have not escaped after six iterates of F, as a function of their left boundary. Each box is magnified in the subsequent plot.

from the following formula, e.g. [19,20]

$$D_{\rm c} = \lim_{\epsilon \to 0} \frac{\log N(\epsilon)}{\log(1/\epsilon)}, \tag{66}$$

where N is the minimal number of the intervals of length ϵ, needed to cover the set. To calculate $D_{\rm c}$ we approximate the set A by iterating the interval $[0,1]$ and by removing all those x, which after n iterations leave the domain of F, i.e. escape in one of the intervals J_k. Denote the rest of $[0,1]$ by $A_n \equiv [0,1] \setminus \bigcup_{m=0}^{n} F^{-m}\left(\bigcup J_k\right) = \{(x_i, x_i + \Delta x_i)\}_{i=1}^{N_s}$, so that $A = \lim_{n\to\infty} A_n$. The distribution of segment lengths Δx_i (N_s is their total number) of the set remained after six iterations A_6 is shown in Fig.9 as a function of the left boundary of each segment. The iterations A_n cannot be continued beyond certain $n = n_{\max}$, because of the limited computation accuracy. Since the map $F(x)$ expands phase space very quickly (see Eq.(65)), errors in the calculation of the points from invariant set of F will rapidly grow and after a few iterations the point escapes into one of the intervals J_k just due to insufficient accuracy. Therefore, for numerical purposes we consider the sets A_n with $n = 5, 6, 7$. After $n \gtrsim 8$ iterates the number of segments N_s in A_n starts to decrease for

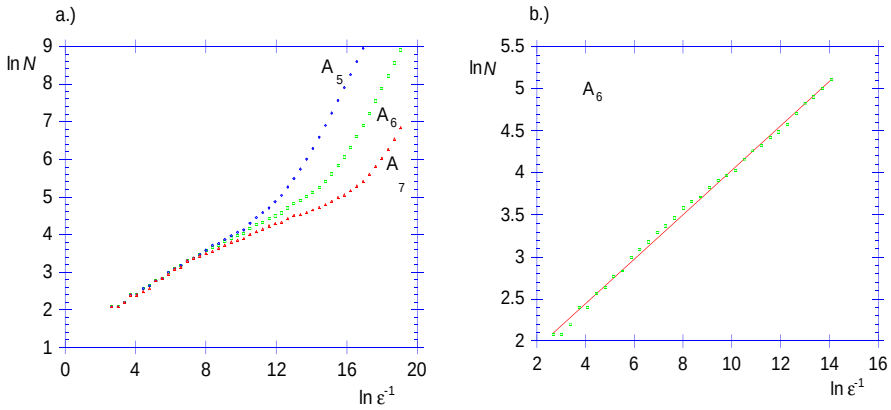

Fig. 10. a.) The number of intervals needed to cover the sets A_n for $n = 5, 6, 7$ and for $\lambda = 0.3$, $\beta = 1.3$ b.) A linear fit to $\ln N$ for the case $n = 6$.

above reasons. The dependence $N(\epsilon)$ for different A_n is shown in Fig.10. Since A_n is measure one for any finite n , even though very irregular, the dependence $N(\epsilon)$ becomes $N \sim \epsilon^{-1}$ for ϵ smaller than typical segment length in A_n. At larger ϵ one can see a distinct region of the linear behavior in the $\log - \log$ scale, which captures the main fractal properties of the limiting $(n \to \infty)$ set A. In this ϵ- range the slopes of the curves are essentially identical for $4 < n < 8$. The transition to the $D_c = 1$ behavior at smaller ϵ occurs earlier for smaller n which is a natural result. For $n \geq 8$ the slope becomes smaller, which underestimats the capacity dimension of set A due to the escape of points from A_n because of the limited computation accuracy. For $\lambda = 0.3$ and $\beta = 1.3$ the capacity dimension $D_c \approx 0.26$.

6 Comparison with the time dependent numerical solutions

Before we verify numerically some of our above results it is worthwhile to comment on the possible approaches to this verification. First of all there are two different aspects of our analytic calculations. One of them concerns the response of damped nonlinear oscillator (5) to the large amplitude forcing. In the present paper we leave aside the problem of numerical study of (5) regarding its reduction to the discrete map (60). We only note here that such a study would not be straightforward, since the typical fixed point of this map is unstable as well as the motion on the repellor, considered in the previous section and the solutions of (5) are unbounded in their vast majority. Backward iterations of this map, locally attracted by this fixed points, would require a choice of preimages, i.e. the branches of $F^{-1}(x)$, since $F(x)$ is not invertible. Even though this numerical study were successively done, it would not give us an ultimate answer to an important question concerning the driven KdVB equation. In particular, it would be still unclear which solutions of the

travelling wave type, i.e. the solutions of (5) are the attractors of Eq.(1)? We therefore perform direct integration of the evolution equation (1) in time. It should be realized, however, that this approach is also insufficient for a firm manifestation of spatial chaos, since it would require an infinite number of modes or equivalently an infinitely long system. An additional problem is that we already have two essentially different scales (dispersion/viscosity and the driver scales) and in order to detect at least a possible trend to the spatially chaotic behavior we would need to model a system that appreciably exceeds the driver scale. Note, that it is the shock-train technique, developed in the previous sections that is especially suitable for handling systems with considerably different spatial scales. At the same time, the spatially chaotic travelling wave solutions, obtained in the preceeding sections are not necesseraly the attractors of time dependent Eq.(1). An example of the impossibility of chaotic solutions is given in [21] where the Frenkel-Kontorova model is considered. In particular, it was proven in [21], that the ground-states of this model can be periodic or quasi-periodic but the spatial chaos is ruled out.

The numerical investigation of the onset of spatial chaos is beyond the scope of this paper. The above arguments suggest that it could be a rather difficult task and certainly deserves a separate study. First of all one should check whether at least the first steps in a route to spatial chaos can be described correctly by an analytical shock-train solution obtained in previous sections. A possible strategy consists of obtaining 2π periodic solutions numericallly and of further identification them with the correspondent fixed points of the map $F(x)$ (sec.4). Then, the 4π-periodic solutions should be found and identified with the fixed points of $F^2 \equiv F \circ F$. These fixed points appear in the vicinities of the unstable fixed points of F. A continuation of this process should in principle give rise to the spatially chaotic solutions. This section deals with the very begining of this program. First, we demonstrate that the travelling wave solutions of (5) do attract time dependent solutions of Eq.(1). Second, an approximate Poincaré map can really capture their complexity.

We start with the numerical integration of Eq.(1) for periodic driver given by Eq.(63) with different initial conditions. The results are shown in Figs.11. One can see from these two figures that the shock-train is a persistent solution of Eq.(1). Starting from large amplitude sinusoidal profile (Fig.11a), the solution steepens very quickly and forms a shock-train which has the driver period. Fig.11b demonstrates the case with completely different initial condition, where a rather random small amplitude perturbation is imposed. It decays rapidly due to the dispersive spreading and viscosity. Then after the amplitude of the driver's harmonic achieved nonlinear level, it steepens to form exactly the same travelling wave solution. Figs.12 show the comparison of such a steady state with an asymptotic solution given by the formulae (17,21-23). It is seen from Fig.12a that the agreement is very good, taking into account that only zero order solution $u_0(\xi, x)$ is plotted. There are, how-

Fig. 11. Formation of the shock-train for two different initial conditions, and the driver given by Eq.(63) The coordinate is shifted back by $\pi/2$ and compressed to $[0, 1]$. Only one period of the solution is shown.

ever, two regions where the deviation is significant. They correspond to the nonuniformities of the asymptotic solution (17), resolved in secs.2 and 3, but not taken into account in Figs.12 for simplicity. First, the amplitude of the first peak is somewhat larger than numerical one due to our replacement x'_* by x_*, which overestimates $k(x)$ at $x \simeq x_*$ (see sec.2). Second, the deviation in the region where an oscillatory behavior is changed for a monotonic one results simply from invalidity of $u_0(\xi, x)$ given by formula (17) at the turning point x_0 (sect.3) in the case of moderate β. (We have taken $\beta = 1.8$ to obtain pronounced solitons between the shock and the turning point x_0). Thus, the agreement can be even improved by using the asymptotics given in sec.2,3 instead of Eq.(17).

The solution $u_0(\xi, x)$ depends also on additional parameter, the shock coordinate x_*. For the period-one solutions considered here, x_* must be equal to one of the fixed points of the map $F(x)$, plotted in Fig.12b. In the analytical solution shown in Fig.12a, $x_* = 0.497$ which corresponds to the filled circle in Fig.12b. Solutions corresponding to the empty circles in Fig.12b are shown in Fig.12c and they clearly do not agree with the numerical solution. This allows us to identify a continuous solution with one of the discrete shock coordinates. There are as many as twenty fixed points of the map $F(x)$ shown in Fig.12b. Each of them corresponds to a period-one solution of the driven KdVB equation. Moreover, one can easily draw $F^n(x)$ for $n > 1$ and obtain, in principle, all the solutions of period n, as the fixed points of F^n. Due to the limitations of applied asymptotic method, a few right most fixed points cannot be described correctly. At the same time they correspond to the solution, in which $u \sim \sqrt{Q}$ throughout the driver period, i.e. actually to the counterpart of the solution $u \sim -\sqrt{Q}$ briefly discussed in sec.4.2. This situation can in principle be systematically improved by adopting an appropriate asymptotic method for these solutions, which would allow us to incorporate them in to the shock train class simply as limiting solutions with the vanishing shock amplitude.

The fixed points of the map $F(x)$ produce a discrete set of 2π-periodic solutions. Each solution contains an integral number of solitons that gradually decrease in amplitude filling up the region between the shock front and the turning point. Why does the system follow the solution with $x_* = 0.497$? It is clear that the system choose a steady state to follow according to the constraints imposed by the initial conditions. Such a constraint is the mass

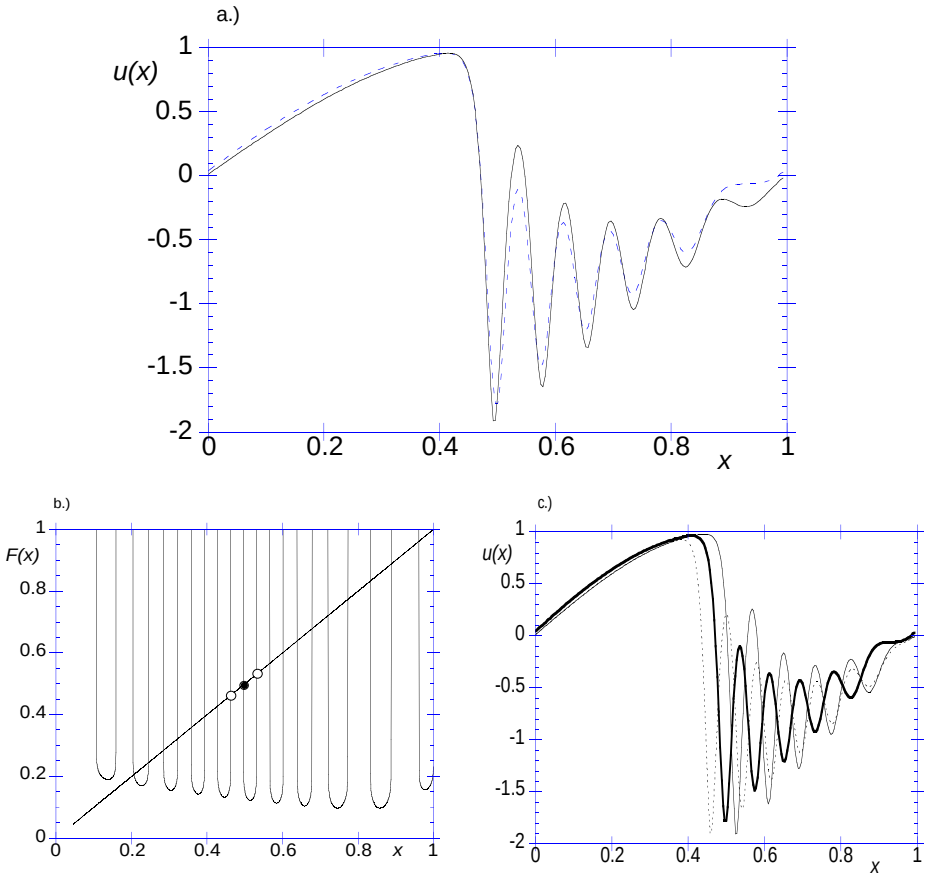

Fig. 12. a.) Zeroth order analytic solution Eq.(17) (solid line) having the shock at $x_* = 0.497$ (the correspondent fixed point of the map $F(x)$ is marked by the filled circle in Fig.12b). Dashed line shows the steady state numerical solution. Both curves are drawn for the case $\lambda = 0.1$ and $\beta = 1.8$.
b.) The map $F(x)$ for the same λ and β. c.) The same numerical solution as in Fig.12a (heavy line) and the two analytical solutions (thin and dotted lines) having shocks at x_* marked by the opened circles in Fig.12b.

invariant

$$\bar{u} = \int_0^1 u(x, t = 0)dx, \tag{67}$$

which was set to zero. In order to estimate $\bar{u}$ from the lowest order solution (17), we can to the good approximation average the fast oscillations and regard k as a small value for $x > x_*$. The solution $u_0\left(\xi(x_*, x), x\right)$ will then produce $\bar{u} = 0$ only for $x_* = 1/2$. For arbitrary $\bar{u}$-value, the system follows the solution with an appropriate x_*-value. It is interesting to note that a solution taken from the set $u_0\left(\xi(x_n, x), x\right)$, being discrete fulfills the condition $\bar{u} = 0$ only

approximately, although with a good accuracy $\sim \lambda \ll 1$ (here x_n is one of the fixed points of $F(x)$). Thus, the difference might in principle be compensated by the higher order terms. We do not consider this problem here. More detailed comparison of our analytical solutions with the numerical ones including the doublings of the spatial period will be done in a future paper.

7 Discussion

An interesting feature of the repellor considered in sec.5.2 consists in the concentration of its natural measure inside narrow intervals where $F'(x) \gg 1$. The function $F(x)$ maps these intervals onto the appreciable part of $[0, 1]$ and, therefore, those are the points from these intervals which have better chances to avoid the escape set $J_{\rm k}$ after a number of iterates. All the unstable fixed points, shown in Fig.12b belong to these intervals. Motion on the repellor is essentially a random walk between these narrow intervals. If we neglect their width together with the underlying multifractal structure of these intervals, we obtain a discretization of the shock coordinates in the shock-train. The meaning of such a discretization is obvious; it corresponds to an integral number of vibrations or solitons between the shock coordinate and the turning point x_0. These regions of oscillatory behaviour can also be considered as optically transparent domains, created nonlinearly by the driver ("potential wells"). This can be easily understood from the consideration of the solution near the turning point x_0, where the small amplitude oscillations allow the linear treatment (sec.3). Figs.12b,c in particular demonstrate that at each second fixed point of $F(x)$ the number of solitons differs by unity. Note, that the majority of the fixed points are close to zeroes of function $f(x)$ in Eq.(60). This fact suggests a simplified "quantization rule" for the discrete shock coordinate x_* in the shock-train (which is valid for sufficiently small $g(x)$)

$$\int\limits_{x_*}^{x_0} \frac{Q_0^{1/4} dx}{\mathbf{K}(x)(k^2 + k'^4)^{1/4}} = \sqrt{2}\lambda \left(n + \frac{1}{4}\right) \tag{68}$$

In general, even when the parameter β is not large and the linear approximation at the turning point x_0 is not justified, the number of solitons is a constitutive aspect of the considered chaos scenario. To put it anotherway, consider the motion on the invariant set of the map $F(x)$. Suppose we know the coordinate x_* of some reference shock in the shock-train or, equivalently, the coordinate of the leftmost soliton in the correspondent potential well. An appropriate accuracy to which x_* should be known is $o(\lambda)$, as Eq.(68) suggests. In practice, that would be enough only for identifying x_* with one of the region of the concentration of the natural measure, marked by the digits in Fig.9a. Better accuracy in shock coordinate would allow us to go only few

steps deeper into coarsegraining of this region. Since the Lyapunov exponents are typically of order of $1/\lambda$ on the repellor, we cannot even predict into which region falls the coordinate of the next shock in the shock-train. With a more accurate knowledge of the reference shock coordinate we could at best predict a few next. Therefore we will obtain an apparently random sequence of soliton numbers in the subsequent potential wells, created by fully deterministic driver. In general, one can argue in terms of the topological conjugacy between these random sequences and the set of real numbers, as it is widely used in study of deterministic chaos in quadratic or binary tent maps, see e.g. [22,23]. The number of the coarsegrained intervals in Fig.9a or, equivalently, the number of solutions of Eq.(68) for x_* can be taken as a base of arithmetic.

8 Conclusions

Using asymptotic methods we have represented the continuous travelling wave solutions of the periodically driven KdV-Burgers equation as a Poincaré map at the driver period. Unlike many other analytical approaches to driven equations, the amplitude of the driver is not assumed to be small. We argue that the typical response of this system to the external force consists of a fragmentation of the solution into two alternating parts. One of them is smooth and has the driver scale. The second is an oscillatory one (shock), its scale is defined by the small dispersion and viscosity. The scenario of the spatial chaotization of this solution is suggested. It consists in a randomization of the shock-coordinate with respect to the driver phase under the action of the derived Poincaré map.

Acknowledgements. The author wish to express special thanks to T. Hada, A.I. Neishtadt, C.F. Kennel and C.C. Wu for interesting discussions. Fruitful discussions with H.D.I. Abarbanel and the other participants of a seminar at the Institute for Nonlinear Sciences, La Jolla, as well as with F.H. Busse and the participants of his seminar at the Bayreuth university are gratefully acknowledged. This work was supported by National Science Foundation Grant No. PHY 91-20591 and by the International Project "Wave Chaos" sponsored by the Government of the Russian Federation.

References

[1] S. Leibovich and A. R. Seebas (Eds.) in: Nonlinear waves, Ithaca: Cornell University press, 1974.

[2] V.I. Karpman, Nonlinear waves in dispersive media, Nauka, Moscow, 1973 (in russian).

[3] R.Z. Sagdeev, D.A. Usikov and G.M. Zaslavsky, Nonlinear Physics, Harwood, Chur, 1988.

[4] G. B. Whitham, Linear and nonlinear waves Wiley, New York, 1974.

[5] A.V. Gurevich, L.P. Pitaevskii, JETP 38 (1974) 291.

[6] C. F. Kennel, M. A. Malkov, R. Z. Sagdeev, V. D. Shapiro, and A. V. Khrabrov, Sov. Phys. JETP Lett. 48 (1988) 79.

[7] M.A. Malkov, C.F. Kennel, C.C. Wu, R. Pellat and V.D. Shapiro, Phys. Fluids B 3 (6), (1991), 1407.

[8] A. Rogister, Phys. Fluids 14 (1971) 2733.

[9] M.A. Malkov, R.Z. Sagdeev and V.D. Shapiro, Phys. Lett. A 151 (1990) 505

[10] M.A. Malkov, A.D. Kotelnikov and C.F. Kennel, Physica 86D (1995) 480.

[11] T. Taniuti, J. Phys. Soc. Japan, 56 (1986) 1286 .

[12] H. Moriguchi, K.Nozaki and T. Taniuti, J. Phys. Soc. Japan 57 (1988) 470.

[13] E.N. Lorenz, J. Atmos. sci., 20 (1963) 130.

[14] T. Hada, C.F. Kennel, B. Buti and E. Mjolhus, Phys. Fluids B 2 (1990) 2581.

[15] G.B. Whitham, Proc. Roy. Soc A283 (1965) 238.

[16] M. V. Fedorjuk, Asymptotic methods for linear differential equations Nauka, Moscow 1983 (in russian).

[17] M.J. Feigenbaum, J. Stat. Phys. 19 (1978) 25.

[18] Y. Pomeau and P. Maneville, Comm. Math. Phys. 74 (1980) 189.

[19] J. D. Farmer, E.Ott and A. Yorke, Physica 7D (1983) 153.

[20] H. Kantz and P.Grassberger, Physica 17D (1985) 75.

[21] S. Aubry and P.Y. Le Daeron, Physica 8D (1983) 381.

[22] R.L. Devaney, An Introduction to chaotic dynamical systems, Adison-Wesley 1989

[23] J.L. McCauley, Chaos, dynamics, and fractals, Cambridge University Press, 1993.